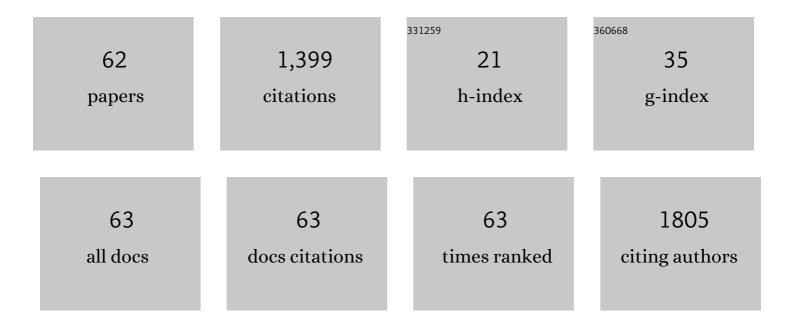
Andrew D Parsekian

List of Publications by Year in descending order

Source: https://exaly.com/author-pdf/34945/publications.pdf Version: 2024-02-01



#	Article	IF	CITATIONS
1	Multiscale geophysical imaging of the critical zone. Reviews of Geophysics, 2015, 53, 1-26.	9.0	192
2	Threshold sensitivity of shallow Arctic lakes and sublake permafrost to changing winter climate. Geophysical Research Letters, 2016, 43, 6358-6365.	1.5	68
3	Inference of the impact of wildfire on permafrost and active layer thickness in a discontinuous permafrost region using the remotely sensed active layer thickness (ReSALT) algorithm. Environmental Research Letters, 2019, 14, 035007.	2.2	64
4	Uncertainty in Peat Volume and Soil Carbon Estimated Using Groundâ€Penetrating Radar and Probing. Soil Science Society of America Journal, 2012, 76, 1911-1918.	1.2	63
5	Remotely Sensed Active Layer Thickness (ReSALT) at Barrow, Alaska Using Interferometric Synthetic Aperture Radar. Remote Sensing, 2015, 7, 3735-3759.	1.8	59
6	Estimating the water holding capacity of the critical zone using nearâ€surface geophysics. Hydrological Processes, 2018, 32, 3308-3326.	1.1	59
7	Seasonal thaw settlement at drained thermokarst lake basins, Arctic Alaska. Cryosphere, 2014, 8, 815-826.	1.5	50
8	<scp>NMR</scp> Logging to Estimate Hydraulic Conductivity in Unconsolidated Aquifers. Ground Water, 2016, 54, 104-114.	0.7	49
9	Detecting unfrozen sediments below thermokarst lakes with surface nuclear magnetic resonance. Geophysical Research Letters, 2013, 40, 535-540.	1.5	45
10	Lake and drained lake basin systems in lowland permafrost regions. Nature Reviews Earth & Environment, 2022, 3, 85-98.	12.2	41
11	Quantifying landscape morphology influence on peatland lateral expansion using groundâ€penetrating radar (GPR) and peat core analysis. Journal of Geophysical Research G: Biogeosciences, 2013, 118, 373-384.	1.3	39
12	Active layer thickness as a function of soil water content. Environmental Research Letters, 2021, 16, 055028.	2.2	35
13	Presence of rapidly degrading permafrost plateaus in south-central Alaska. Cryosphere, 2016, 10, 2673-2692.	1.5	34
14	Geophysical Measurements to Determine the Hydrologic Partitioning of Snowmelt on a Snowâ€Đominated Subalpine Hillslope. Water Resources Research, 2018, 54, 3788-3808.	1.7	32
15	Identifying historical and future potential lake drainage events on the western Arctic coastal plain of Alaska. Permafrost and Periglacial Processes, 2020, 31, 110-127.	1.5	30
16	The effect of peat structure on the spatial distribution of biogenic gases within bogs. Hydrological Processes, 2014, 28, 5483-5494.	1.1	29
17	Hydraulic Conductivity Calibration of Logging NMR in a Granite Aquifer, Laramie Range, Wyoming. Ground Water, 2019, 57, 303-319.	0.7	29
18	Variations in freeâ€phase gases in peat landforms determined by groundâ€penetrating radar. Journal of Geophysical Research. 2010. 115	3.3	28

ANDREW D PARSEKIAN

#	Article	IF	CITATIONS
19	Comparing Measurement Response and Inverted Results of Electrical Resistivity Tomography Instruments. Journal of Environmental and Engineering Geophysics, 2017, 22, 249-266.	1.0	27
20	Application of groundâ€penetrating radar to measure nearâ€saturation soil water content in peat soils. Water Resources Research, 2012, 48, .	1.7	26
21	Observing Heterogeneous Unsaturated Flow at the Hillslope Scale Using Time‣apse Electrical Resistivity Tomography. Vadose Zone Journal, 2019, 18, 1-16.	1.3	24
22	Geophysical evidence for the lateral distribution of free phase gas at the peat basin scale in a large northern peatland. Journal of Geophysical Research, 2011, 116, .	3.3	21
23	Expansion rate and geometry of floating vegetation mats on the margins of thermokarst lakes, northern Seward Peninsula, Alaska, USA. Earth Surface Processes and Landforms, 2011, 36, 1889-1897.	1.2	21
24	Uncertainty estimates for surface nuclear magnetic resonance water content and relaxation time profiles from bootstrap statistics. Journal of Applied Geophysics, 2015, 119, 61-70.	0.9	21
25	Transient Electromagnetic Surveys for the Determination of Talik Depth and Geometry Beneath Thermokarst Lakes. Journal of Geophysical Research: Solid Earth, 2018, 123, 9310-9323.	1.4	21
26	Characterizing Heterogeneity in Infiltration Rates During Managed Aquifer Recharge. Ground Water, 2016, 54, 818-829.	0.7	20
27	Geophysical and Hydrochemical Identification of Flow Paths with Implications for Water Quality at an <scp>ARR</scp> Site. Ground Water Monitoring and Remediation, 2014, 34, 105-116.	0.6	19
28	Bootstrap Calibration and Uncertainty Estimation of Downhole <scp>NMR</scp> Hydraulic Conductivity Estimates in an Unconsolidated Aquifer. Ground Water, 2015, 53, 111-121.	0.7	19
29	Characterizing the Critical Zone Using Borehole and Surface Nuclear Magnetic Resonance. Vadose Zone Journal, 2019, 18, 1-18.	1.3	19
30	Plant Hydraulic Stress Explained Tree Mortality and Tree Size Explained Beetle Attack in a Mixed Conifer Forest. Journal of Geophysical Research G: Biogeosciences, 2019, 124, 3555-3568.	1.3	16
31	Ground-penetrating radar-derived measurements of active-layer thickness on the landscape scale with sparse calibration at Toolik and Happy Valley, Alaska. Geophysics, 2016, 81, H9-H19.	1.4	14
32	Estimating active layer thickness and volumetric water content from ground penetrating radar measurements in Barrow, Alaska. Geoscience Data Journal, 2017, 4, 72-79.	1.8	14
33	Why Are Some Rocky Mountain Lakes Ephemeral?. Water Resources Research, 2018, 54, 5245-5263.	1.7	13
34	Surface nuclear magnetic resonance observations of permafrost thaw below floating, bedfast, and transitional ice lakes. Geophysics, 2019, 84, EN33-EN45.	1.4	13
35	Uniform and lateral preferential flows under flood irrigation at field scale. Hydrological Processes, 2019, 33, 2131-2147.	1.1	12
36	Contrasting lake ice responses to winter climate indicate future variability and trends on the Alaskan Arctic Coastal Plain. Environmental Research Letters, 2018, 13, 125001.	2.2	11

#	Article	IF	CITATIONS
37	Parameterization of a hydrologic model with geophysical data to simulate observed subsurface return flow paths. Vadose Zone Journal, 2020, 19, e20024.	1.3	11
38	Permafrost Dynamics Observatory—Part I: Postprocessing and Calibration Methods of UAVSAR Lâ€Band InSAR Data for Seasonal Subsidence Estimation. Earth and Space Science, 2021, 8, e2020EA001630.	1.1	11
39	Inverse Methods to Improve Accuracy of Water Content Estimates from Multi-offset GPR. Journal of Environmental and Engineering Geophysics, 2018, 23, 349-361.	1.0	11
40	Geophysical Observations of Taliks Below Drained Lake Basins on the Arctic Coastal Plain of Alaska. Journal of Geophysical Research: Solid Earth, 2021, 126, e2020JB020889.	1.4	9
41	Validation of Permafrost Active Layer Estimates from Airborne SAR Observations. Remote Sensing, 2021, 13, 2876.	1.8	9
42	Symmetry based frequency domain processing to remove harmonic noise from surface nuclear magnetic resonance measurements. Geophysical Journal International, 2017, 208, 724-736.	1.0	8
43	Influence of permafrost thaw on an extreme geologic methane seep. Permafrost and Periglacial Processes, 2021, 32, 484-502.	1.5	8
44	Remote Sensing-Based Statistical Approach for Defining Drained Lake Basins in a Continuous Permafrost Region, North Slope of Alaska. Remote Sensing, 2021, 13, 2539.	1.8	8
45	Hydrogeophysical Inversion of Timeâ€Lapse ERT Data to Determine Hillslope Subsurface Hydraulic Properties. Water Resources Research, 2022, 58, .	1.7	7
46	Small Root Biomass Effect on the Dielectric Properties of Soil. Vadose Zone Journal, 2012, 11, .	1.3	5
47	Hydrogeophysical comparison of hillslope critical zone architecture for different geologic substrates. Geophysics, 2021, 86, WB87-WB107.	1.4	5
48	A new Stefan equation to characterize the evolution of thermokarst lake and talik geometry. Cryosphere, 2022, 16, 1247-1264.	1.5	5
49	Estimating winter ebullition bubble volume in lake ice using ground-penetrating radar. Geophysics, 2018, 83, H13-H25.	1.4	4
50	Field scale quantification indicates potential for variability in return flows from flood irrigation in the high altitude western US. Agricultural Water Management, 2020, 232, 106062.	2.4	4
51	Ground-penetrating radar-derived measurements of active-layer thickness on the landscape scale with sparse calibration at Toolik and Happy Valley, Alaska. Geophysics, 2016, 81, H1-H11.	1.4	3
52	Spatial snowdrift modelling for an open natural terrain using a physicallyâ€based linear particle distribution equation. Hydrological Processes, 2022, 36, .	1.1	3
53	Geostatistical Rock Physics Inversion for Predicting the Spatial Distribution of Porosity and Saturation in the Critical Zone. Mathematical Geosciences, 2022, 54, 1315-1345.	1.4	3
54	Near-surface geophysics for informed water-management decisions in the Aṉangu Pitjantjatjara Yankunytjatjara (APY) lands of South Australia. The Leading Edge, 2014, 33, 1342-1347.	0.4	2

ANDREW D PARSEKIAN

#	Article	IF	CITATIONS
55	Hydrogeophysics for Informed Water Management Decisions in the Anangu Pitjantjatjara Yankunytjatjara (APY) Lands of South Australia. ASEG Extended Abstracts, 2015, 2015, 1-3.	0.1	2
56	Advancements in the measurement of the cryosphere using geophysics — Introduction. Geophysics, 2016, 81, WAi-WAii.	1.4	2
57	The state of the science and vision of the future: Report from the Hydrogeophysics Workshop. The Leading Edge, 2013, 32, 814-818.	0.4	1
58	Joint Retrieval of Soil Moisture and Permafrost Active Layer Thickness Using L-Band Insar and P-Band Polsar. , 2020, , .		1
59	Hydrogeophysics — Introduction. Geophysics, 2021, 86, WBi-WBii.	1.4	0
60	Permafrost Dynamics Observatory: Retrieval of Active Layer Thickness and Soil Moisture from Airborne Insar and Polsar Data. , 2021, , .		0
61	Calibrating surface NMR hydraulic conductivity estimates using logging NMR and direct hydraulic conductivity measurements. , 2013, , .		0
62	Surface NMR to Image Aquifer Properties in a Magnetic Subsurface. ASEG Extended Abstracts, 2015, 2015, 1-5.	0.1	0